Reactivity of *Z* and *E* Isomers, Growing Chain Isomerization, and Chain Transfer Reactions in Ethene/2-Butene Copolymerization by Metallocene-Based Catalysts

Pasquale Longo,*,† Fabia Grisi,† Gaetano Guerra,† and Luigi Cavallo‡

Dipartimento di Chimica, Università di Salerno, 84081 Baronissi (SA), Italy; Dipartimento di Chimica, Università di Napoli, Via Mezzocannone 4, I-80134 Napoli, Italy

Received December 31, 1999; Revised Manuscript Received April 12, 2000

ABSTRACT: Copolymerization of *Z* and *E* isomers of 2-butene with ethene, in the presence of catalytic systems based on C_{2v}-, C_s-, and C_2-symmetric group 4 *ansa*-metallocenes is investigated. Higher reactivities of *Z* and *E* isomers of 2-butene, in the presence of C_2- and C_s-symmetric metallocenes, respectively, are predicted by molecular modeling and are proved by polymerization tests relative to pure isomers as well as to mixtures of them. The copolymerization experiments have also shown that both growing chain isomerizations and chain transfer reactions are dependent on the configuration (*Z* or *E*) of 2-butene while are independent of the metallocene symmetry. To account for this behavior, isomerization mechanisms involving intermediates with metal−allyl bonds are suggested. Possible mechanisms of chain transfer reactions are also discussed.

1. Introduction

Different kinds of homogeneous catalysts based on group 4 metallocene/methylalumoxane (MAO) systems have been discovered.[1−5] Depending on the symmetry of the metallocene, these systems present completely different stereospecific behaviors. For instance, catalytic systems based on stereorigid C_2-symmetric metallocenes comprising π-ligands such as ethenebis(1-indenyl) or ethenebis (4,5,6,7-tetrahydro-1-indenyl) polymerize 1-alkenes to isotactic polymers with a non-Bernoullian distribution of steric defects, consistent with chiral site stereocontrol.[1−3] On the other hand, catalytic systems based on stereorigid C_s-symmetric metallocenes comprising π-ligands such as isopropyl(cyclopentadienyl)-(9-fluorenyl) polymerize 1-alkenes to syndiotactic polymers, again consistently with a prevailingly chiral site stereocontrol.[4,5] Moreover, catalytic systems comprising metallocene C_{2v}-symmetric ligands, like bis(cyclopentadienyl) or the bridged dimethylsilylbis(cyclopentadienyl), generally polymerize 1-alkenes to essentially atactic polymers.[1]

The stereoselectivity of each monomer insertion step is a necessary (but not sufficient) prerequisite for stereospecific catalytic systems. Molecular modeling studies relative to several metallocenes have shown that when a substantial stereoselectivity is calculated for primary propene insertion, this is mainly due to steric interactions between the methyl group of the chirally coordinated monomer with the chirally oriented growing chain.[6−10] According to this *growing chain chiral orientation mechanism*, which was previously proposed for the classical heterogeneous Ziegler−Natta catalysts,[11,12] the *stereoselectivity* of these models stems from direct interactions of the π-ligands with the growing chain, determining its chiral orientation which, in turn, discriminates between the two prochiral faces of the monomer, and is not due to direct interactions of the π-ligands with the monomer.[6−12]

This mechanism of stereoselectivity is in agreement with the available experimental data. In this respect, it may be of interest to recall that a relevant experimental proof of the importance of the role played by the growing chain in determining the steric course of the insertion reaction was given, by Zambelli and coworkers, by the observation of the stereospecificity in the first step of polymerization.[13−16] This stereoselective mechanism is also in accordance with the elegant analysis and optical activity measurements by Pino et al.[17] on the saturated propene oligomers obtained, under suitable conditions, with this kind of catalyst, proving that the *re* insertion of the monomer is favored in the case of (*R*,*R*) chirality of coordination of the bis(indenyl) ligand. Moreover, also the presence of opposite stereoselectivities in deuteration and oligomerization[18] have been rationalized in terms of the proposed stereoselective mechanism.[17−19]

For a given catalytic model, the stereoselectivity of each insertion step does not ensure its stereospecificity. In fact, the possible presence, as well as the kind, of *stereospecificity* depends on possible differences between stereostructures of transition states of two successive insertion steps. In fact, in the framework of the chain migratory insertion mechanism,[1,20,21] the stereospecific behavior of the model sites depends on the relationship between the two situations obtained by exchanging the relative positions of the growing chain and of the incoming monomer. Depending on the local symmetry of the coordinated bridged π ligand, these two situations are identical or enantiomeric for C_2- or C_s-symmetric metallocenes such as those previously described, respectively. These model sites, if the insertion step is stereoselective, are consequently isospecific and syndiospecific, respectively.[1−12]

Molecular mechanics analyses have been able to rationalize not only the stereoselectivity (and stereospecificity) of regioregular primary insertion steps but also the stereoselectivities relative to occasional secondary monomer insertions as well as relative to primary insertions following these secondary inser-

† Università di Salerno.
‡ Università di Napoli.

10.1021/ma992186w CCC: $19.00
Published on Web 06/07/2000

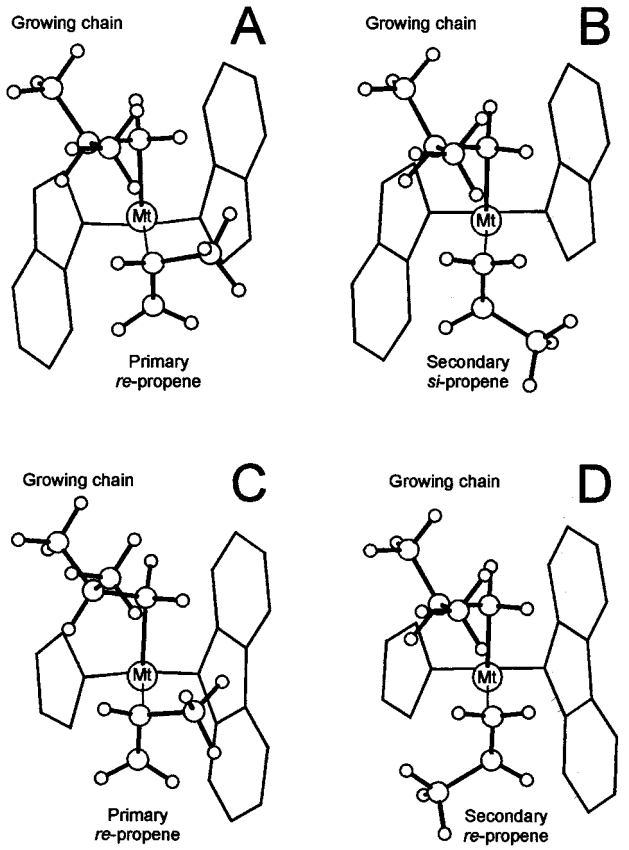

Figure 1. Minimum energy preinsertion intermediates for model catalytic complexes comprising a bridged π-ligand, a propene molecule, and an isobutyl group (simulating a growing primary polypropene chain), taken from ref 22. When the bridged π-ligand presents a local C_2 symmetry axis, opposite propene enantiofaces are favored for primary, A, and secondary, B, insertions. On the contrary, when the bridged π-ligand presents a local C_s symmetry plane, a same propene enantioface is favored for primary, C, and secondary, D, insertions. The shown C_2-symmetric catalyst presents a (*R*,*R*) chirality of coordination of the bis(indenyl) ligand. The considered polymerization step for the C_s-symmetric catalyst presents a *R* chirality at the central metal atom.

tions.[8,22] Typical minimum energy preinsertion intermediates corresponding to primary and secondary propene insertions for models of an isospecific C_2-symmetric and of a syndiospecific C_s-symmetric catalytic system are shown in parts A and B and parts C and D of Figure 1, respectively. In short, the models of Figure 1 show that the *stereoselectivities for primary and secondary propene insertions of isospecific and syndiospecific model sites are in favor of opposite and equal monomer prochiral faces, respectively*.[22,23]

These molecular modeling results are in good agreement with the observed microstructure of polypropene chains obtained by isospecific catalytic systems including the aforementioned as well as analogous bridged π-ligands, indicating stereoselectivities in favor of opposite monomer enantiofaces for primary and secondary insertions.[24,25] As for syndiospecific catalytic systems based on C_s-symmetric metallocenes, which are highly regioregular,[22,26,27] their stereoselectivity in regioirregular insertions has been experimentally investigated for propene based copolymers only.[26,27] In particular, ^{13}C NMR characterization of ethene−1-^{13}C/propene copolymers suggests that the very low amounts of regioirregular (secondary) propene units (in the range 0.03−0.07%) are substantially stereoirregular.[26] On the contrary, NMR characterization of propene/styrene/ethene terpolymers has shown that insertion of propene (primary) and of styrene (secondary) occur with the same enantioface for syndiospecific C_s symmetric metallocenes,[27b] while they occur with opposite enantiofaces for isospecific C_2 symmetric metallocenes.[27a] It is also worth noting that this stereoselective behavior for primary and secondary insertions is able to account for the lower regiospecificity of isospecific catalytic complexes with respect to syndiospecific and aspecific ones.[22]

Scheme 1

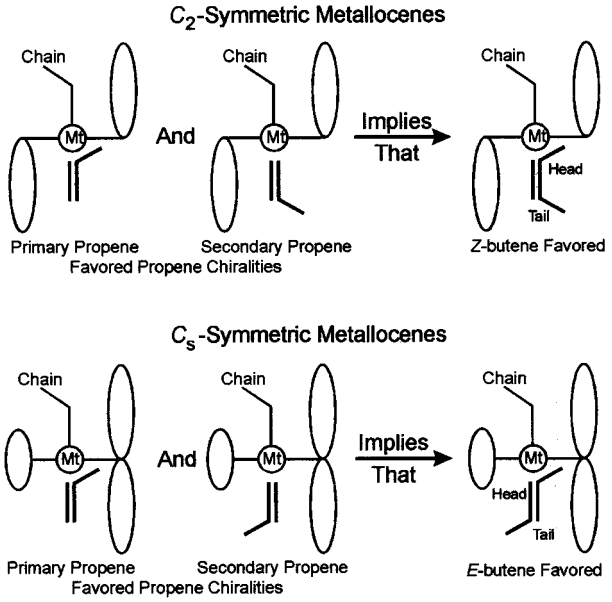

The observation of the minimum energy models of intermediates such as those of Figure 1A−D has suggested to us a possible preferential insertions of *Z* and *E* geometrical stereoisomers of 2-butene, for C_2- and C_s-symmetric catalysts, respectively (see Scheme 1).

It is well-known that, by using heterogeneous and homogeneous Ziegler−Natta catalysts, olefins containing an internal double bond do not yield high molecular weight homopolymers.[28] However, linear high molecular weight copolymers of *Z*- and *E*-butene with ethene have been obtained by Ziegler−Natta catalysts, generally observing higher polymerization rates with the *Z* isomer. In particular, several stereospecific Ziegler−Natta catalytic systems may promote the formation of crystalline ethene/*Z*-butene alternating copolymer,[29] while catalytic systems which are not stereospecific in the polymerization of 1-alkenes promote the formation of amorphous ethene/*Z*-butene alternating copolymers. On the other hand the ethene/*E*-butene copolymers, when obtained, can present only polyethylene crystallinity.[28] Finally, the ability of C_2-symmetric metallocenes to polymerize *Z*-olefins as cyclobutene or norbornene has been proved by Arndt and Kaminsky.[30]

In this paper, copolymerization of *E* and *Z* isomers of 2-butene with ethene, in the presence of C_{2v}-, C_s-, and C_2-symmetric catalytic systems based on metallocenes comprising the dimethylsilylbis(cyclopentadienyl), isopropyl(cyclopentadienyl)(9-fluorenyl), and ethenebis(1-indenyl) ligands, respectively, has been investigated. The copolymerization of 2-butene with ethene in the presence of the C_s- and C_2-symmetric catalytic systems has been theoretically investigated in a previous paper.[31]

In the first section of the paper, molecular modeling results relative to *Z*- and *E*-butene insertions into a polyethene growing chain are presented. In the second section, experimental results relative to copolymerizations with ethene of *E* and *Z* isomers of 2-butene, in the presence of catalytic systems based on the cited metallocenes, are reported. In the final part, the ability of the models to predict and rationalize selectivity and reactivity of metallocene-based catalytic systems in 2-butene−ethene copolymerizations is discussed. Possible mechanisms of growing chain isomerizations and of chain transfer reactions which are compatible with the different chain microstructures observed for the ethene copolymers with *Z*-butene and *E*-butene are also discussed.

2. Molecular Modeling Studies: Models and Methods

Models. The basic assumptions about the polymerization mechanism are as follows. (i) the mechanism is monometallic and the active center comprises a transition metal−carbon bond.[20,21,32] (ii) the mechanism is in two stages: coordination of the olefin to the catalytic site, followed by insertion into the metal−carbon bond.[20,21,32]

As a consequence, the generally assumed models of the alkene-bound intermediates are metal complexes containing a π-coordinated propene molecule, a σ-coordinated alkyl group (simulating a growing chain) and the σ-coordinated ligands of the precursor metallocenes. For the sake of comparison, the molecular modeling calculations have been performed on models bearing the same dimethylsilyl bridge.

The elements of chirality which are relevant for the ethene−2-butene copolymerization are briefly recalled, to indicate the used terminology. First of all, upon coordination, the prochiral *E*-butene gives rise to nonsuperimposable *si*−*si* and *re*−*re* coordinations.[33] On the contrary, coordination of *Z*-butene is achiral. Moreover, since sequences of 2-butene monomeric units are never obtained (see the section 4), the nearest tertiary carbon atom of the growing chain is too far from the catalytic metal atom. Hence this kind of chirality is ignored, and insertion of 2-butene molecules into an ethene-ending growing chain is considered.

A third element of chirality is the chirality of the catalytic site, which in particular can be of two different kinds.

(i) The first is the chirality arising from coordinated ligands, other than the alkene monomer and the growing chain. For metallocenes with prochiral ligands we used the notation (*R*) or (*S*), in parentheses, according to the Cahn−Ingold−Prelog rules[34,35] extended by Schlögl.[36] Without loss of generality, all the calculations here reported refer to models with the (*R*,*R*) chirality of coordination of the dimethylsilylbis(1-indenyl) ligand.

(ii) The second is an intrinsic chirality at the central metal atom, which for tetrahedral or assimilable to tetrahedral situations, can be labeled with the notation *R* or *S*, by the extension of the Cahn−Ingold−Prelog rules, as proposed by Stanley and Baird.[37] This nomenclature has been used to distinguish the alkene-bound intermediates which may arise by exchanging the relative positions of the growing chain and of the incoming monomer.[6−10] In the framework of the chain migratory insertion mechanism this kind of chirality is inverted at each polymerization step. Without loss of generality, all the calculations here reported refer to models with the *R* chirality at the metal atom of complexes based on the dimethylsilyl(cyclopentadienyl)-(9-fluorenyl) ligand.

Scheme 2

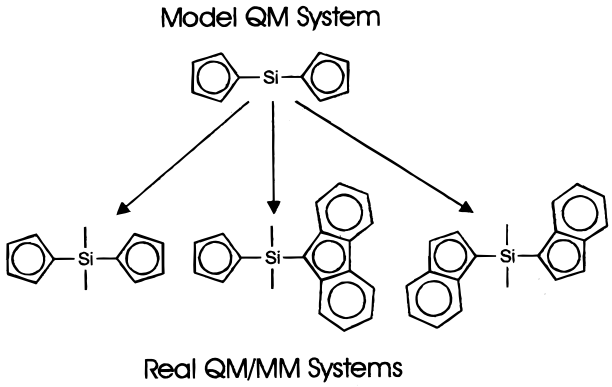

In analogy to previous molecular modeling studies for propene polymerization, it is assumed that the *Z*−*E* selectivity as well as the possible stereoselectivity of *E*-butene insertion are connected with the energy differences between stereoisomeric situations which originate from combination of the above elements of chirality.

Computational Details. Stationary points on the potential energy surface were calculated with the Amsterdam density functional (ADF) program system,[38] developed by Baerends et al.[39,40] The electronic configuration of the molecular systems were described by a triple-ζ basis set on zirconium for 4s, 4p, 4d, 5s, and 5p. Double-ζ STO basis sets were used for silicon (3s,3p), carbon (2s,2p), and hydrogen (1s), augmented with a single 4d, 3d, and 2p function, respectively.[41,42] The inner shells on zirconium (including 3d), silicon (up to 2p) and carbon (1s), were treated within the frozen core approximation. Energetics and geometries were evaluated by using the local exchange-correlation potential by Vosko et al.,[43] augmented in a self-consistent manner with Becke's[44] exchange gradient correction and Perdew's[45,46] correlation gradient correction.

The ADF program was modified by some of us[47−49] to include standard molecular mechanics force fields in such a way that the quantum mechanics (QM) and molecular mechanics (MM) parts are coupled self-consistently, according to the method prescribed by Morokuma and Maseras.[50] The model QM system and the real QM/MM systems are reported in Scheme 2. The partitioning of the systems into QM and MM parts, only involve the skeleton of the catalyst's ligand. Hence, the growing chain, the monomer (either ethene or butene), and the benzene molecule used to model the solvent are always totally composed by pure QM atoms. Moreover, the metal atom, the five-membered Cp rings of all the catalysts, and the $H_2Si<$ bridge connecting the two Cp rings are also composed by pure QM atoms. The only MM atoms, hence, are the methyl groups on the silicon bridge, and the carbon and hydrogen atoms needed to transform the pure QM H_2SiCp_2 skeleton of the ligand into the $Me_2Si(Cp)_2$, $Me_2Si(Cp)(9\text{-}Flu)$ and $Me_2Si(Ind)_2$, ligands. The connection between the QM and MM parts occurs by means of the so-called capping "dummy" hydrogen atoms, which are present in the model system only. These capping atoms are replaced in the real system by the corresponding "linking" carbon atom. For example, the trasformation of the $H_2Si<$ bridge into the $Me_2Si<$ bridge, involves the replacing of the H atoms

of the H_2Si group in the model QM system, with C atoms in the real QM/MM system.

The QM and MM parts are thus linked by the "capping" hydrogen atoms and coupled by van der Waals interactions. The geometry optimization on the whole system was carried out within this coupling scheme between QM and MM atoms. In the optimization of the MM part, the ratio between the Si—C and C—C bonds crossing the QM/MM border, and the corresponding optimized Si—H and C—H distances, were fixed equal to 1.36 and 1.42, respectively. This coupling scheme is described in details in ref 48. Further details on the methodology can be found in previous papers.[47,48]

The molecular mechanics potential developed by Bosnich for bent metallocenes has been adopted.[51] This approach substantially corresponds to an extension of the Karplus's CHARMM force field[52] to include group 4 metallocenes. For the atoms which are involved in reactive events at the active site, we followed the convention that atoms whose type changes during a reaction preserve the original type also in transition state. For example, the ethene and butene sp^2 C atoms have a C sp^2 van der Waals parameter both in the reactant and in the transition state.

All the structures which will follow are stationary points on the combined QM/MM potential surface. Geometry optimizations were terminated if the largest component of the Cartesian gradient was smaller than 0.002 au. Transition states geometries were approached by a linear-transit procedure, using the distance between the C(olefin) and C(chain) atoms which are going to form the new C—C bond as reaction coordinate, while optimizing all other degrees of freedom. Full transition state searches were started from geometries corresponding to maxima along the linear-transit curves. As for geometry optimizations, transition state searches were terminated if the largest component of the Cartesian gradient was smaller than 0.002 au. At the end of each transition state search, the approximated Hessian presented one negative eigenvalue.

3. Molecular Modeling Studies: Results

Alkene-Free Intermediates. The definition of the structure of the alkene-free intermediates, that is of the catalytic complexes at the beginning of each insertion step, is relevant for evaluation of alkene coordination energies and hence for location of possible coordination (alkene-bound) intermediates as well as for evaluation of energy barriers for insertion reactions. The choice of the alkene-free intermediates becomes critical in studies, like the present one, which compare reactivities of different monomers.

The alkene-free intermediates usually assumed for olefin polymerizations by insertion catalysts, present only a σ-bonded (and β-hydrogen agostic bonded) growing chain coordinated to the metal, beside stable ligands. For this kind of intermediates the addition of an alkene monomer to the metal coordination sphere

$$\text{catalyst(chain)} + \text{monomer} \rightarrow \text{catalyst(chain)(monomer)}$$

involves entropy contributions to the free energies of coordination which substantially counterbalance and sometime overcome the attractive enthalpic contributions. Entropy contributions of the order of 40−60 kJ/mol ($T\Delta S$ at 298 K) have been measured[53] or calculated[54,55] for ethene coordination to similar catalyst systems. It is worth noting that these significant entropy contributions generally are not accounted for in modeling studies relative to insertion polymerization catalysis.

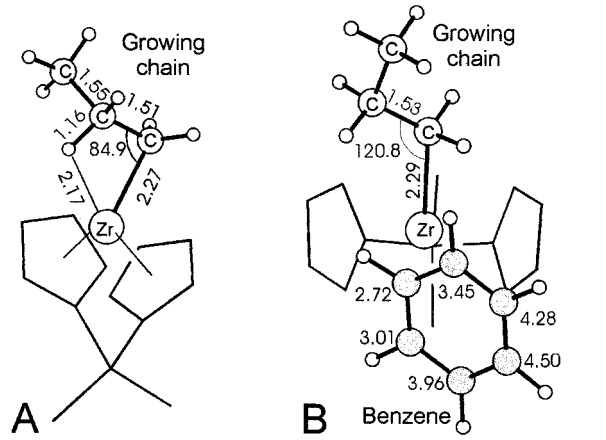

Figure 2. Alkene-free intermediates without, A, and with a coordinated benzene molecule, B, for the considered C_{2v}-symmetric metallocene. The benzene carbon atoms are shaded for clarity, and their distances from the Zr atom, in Å, are indicated.

We here consider models of alkene-free intermediates which also present a solvent molecule coordinated to the metal. Of course, in this assumption the monomer coordination implies a solvent molecule substitution reaction in the metal coordination sphere:

$$\text{catalyst(chain)(solvent)} + \text{monomer} \rightarrow \text{catalyst(chain)(monomer)} + \text{solvent}$$

This way, the entropy changes along the insertion paths are reduced, thus making more reasonable the usual simplifying assumption to ignore the coordination entropy.

The geometries of alkene-free intermediates without and with a coordinated benzene molecule, for the considered C_{2v}-symmetric metallocene, are shown as examples in parts A and B of Figure 2, respectively. The solvent-bound model of Figure 2B is favored by −50 kJ/mol with respect to the solvent-free model of Figure 2A which includes a strong β-hydrogen agostic bond. For the C_s- and C_2-symmetric metallocenes, our calculations indicate that models including a benzene molecule are favored by 32 and 34 kJ/mol, respectively, relative to solvent free models. Hence, alkene-free solvent-bound intermediates are expected to be more realistic for polymerizations conducted in solution. In the following calculations, the alkene-free intermediate including a benzene molecule (like that one of Figure 2B) has been assumed as zero energy situation for each considered catalytic system.

Alkene-Bound Intermediates. The alkene-bound intermediates calculated for ethene, *Z*- and *E*-butene coordination to the considered C_{2v}-symmetric metallocene, are shown in Figure 3, parts A−C, respectively.

The ethene-bound model of Figure 3A (as well as those calculated for the C_s- and C_2-symmetric metallocenes) is very similar to those calculated for other metallocenes.[56,57] The monomer double bond is nearly parallel to the bond connecting the metal to the first carbon of the chain and a very weak α-agostic bond between the growing chain and the metal is formed.

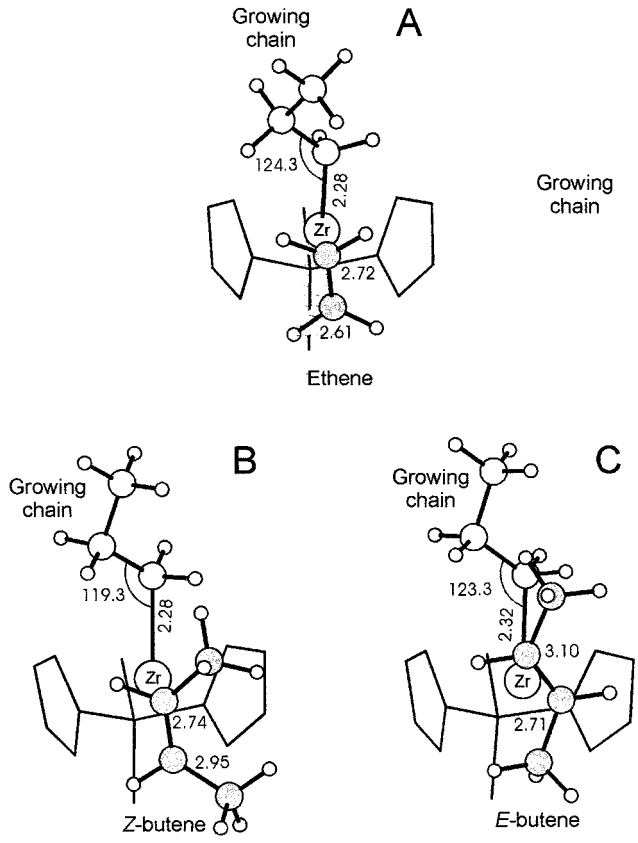

Figure 3. Alkene-bound intermediates calculated for ethene, A, Z−butene, B, and *E*-butene coordination, C, to the considered C_{2v}-symmetric metallocene. The alkene carbon atoms are shaded for clarity.

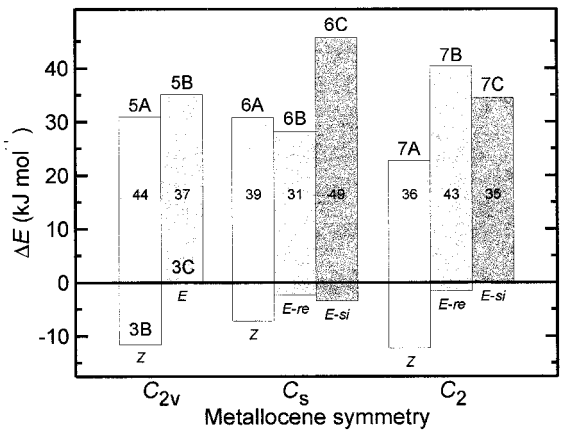

Figure 4. Energies of the alkene-bound intermediates (bottom lines of the bars) and of the transition states (top lines of the bars) for insertion of *Z* and *E* isomers of 2-butene into an ethene ending growing chain, calculated for metallocene catalysts of different symmetries. The zero energy corresponds to the assumed alkene-free (solvent-bound) intermediates. Activation energies, calculated with respect the corresponding alkene-bound intermediates or with respect to the alkene-free intermediate (if lower) are reported inside the bars (in kJ/mol). Bold digits indicate figures showing models of alkene-bound intermediates and transition states. For the C_s-symmetric catalyst, the lower energy transition state for the *E* isomer corresponds to the *re*−*re* (*si*−*si*) enantioface for the insertion step corresponding to the *R* (*S*) chirality at the central metal atom. For the C_2-symmetric catalyst, when the chirality of coordination of the ligand is (*R*,*R*), the lower energy transition state for the *E* isomer corresponds to the *si*−*si* enantioface.

It is worth noting that displacement of the solvent molecule and ethene coordination to form the alkene-bound intermediate is an endothermic process which requires about 8−12 kJ/mol for all the considered metallocenes. Let us recall that, on the contrary, favorable coordination energies close to 30−40 kJ/mol were calculated in previous studies which considered ethene coordination to alkene-free/solvent-free intermediates.[56,57]

For all the considered metallocenes, the 2-butene-bound intermediates present geometries similar to those found for ethene-bound intermediates. However, more favorable uptake energies are calculated both for *Z*- and *E*-butene than for ethene. For instance, for the C_{2v}-symmetric metallocene the *Z*- and *E*-butene uptake energies are roughly 15−20 kJ/mol higher than the ethene uptake energy. The better coordination of 2-butenes with respect to ethene is of course due to the electrodonating effect of the methyl groups.

The coordination of the three monomers on C_s- and C_2-symmetric metallocenes are similar to those calculated for the C_{2v}-symmetric metallocene. However, some minor differences related to their chiralities are observed (bottom lines in Figure 4). In particular, for the C_s-symmetric catalyst, the *Z*-butene alkene-bound intermediate presents a substantial nonbonded interaction between the tail methyl group and a six-membered ring of the fluorenyl ligand, which reduce the coordination energy to nearly 6 kJ/mol. Moreover, for the C_2-symmetric catalyst, the intermediate coordinating *E*-butene with the *si*−*si* enantioface presents substantial nonbonded interactions of the second carbon bond of the growing chain (and its substituents) with a six-membered ring of the indenyl ligand, which make its energy of nearly 5 kJ/mol larger than the energy of the assumed alkene-free intermediate. These kinds of interactions are also present in the corresponding transition states for the insertion reaction and will be discussed in more detail in the next section.

Transition States for Monomer Insertions. Transition states calculated for ethene insertion are very similar to those described in several literature studies, and hence their geometries are not reported here. Let us only note that, in agreement with previous studies, the insertion reaction is substantially barrierless.

On the contrary, transition states calculated for insertion of both 2-butene isomers present substantially higher insertion barriers. The structures of the transition states for insertion of *Z*-butene, *re*−*re* coordinated *E*-butene, and *si*−*si* coordinated *E*-butene into the Zr−C(chain) bond with the C_{2v}-, C_s- and C_2-symmetric metallocenes are reported in Figures 5−7, parts A−C, respectively. The usual four centers transition states involving the metal atom, both sp^2 carbon atoms of the alkene and the first carbon atom of the growing chain is found. Moreover, in the framework of the chiral orientation of the growing chain mechanism,[6−10] for all the obtained transition states the head methyl group of butene is anti relative to the second carbon atom of the growing chain. This feature has been found and described in detail for transition states for primary propene insertion and has a major influence to the stereoselectivity toward α-olefins enantiofaces, both for C_s- and C_2-symmetric metallocene catalysts.[6−10]

The calculated energies of the transition states for *Z*- and *E*-butene insertions relative to the alkene-free (but solvent-bound) species for the three considered catalysts correspond to the top of the bars reported in Figure 4. Activation energies, calculated with respect to the species which is more stable between the corresponding

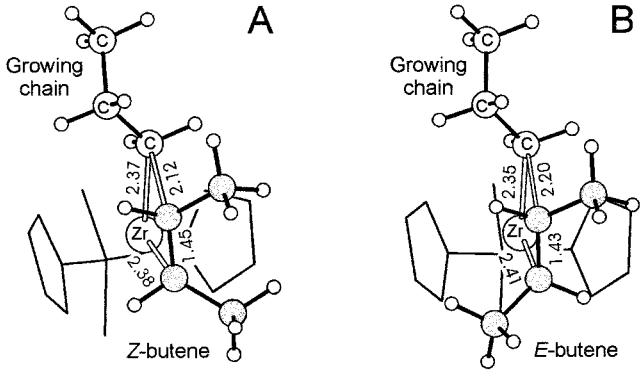

Figure 5. Transition states calculated for the C_{2v}-symmetric metallocene for *Z*-butene, A, and *E*-butene, B. The main bond distances, in Å, are indicated. The alkenes carbon atoms are shaded for clarity.

alkene-bound and alkene-free intermediates correspond to the height of the bars reported in Figure 4. It is worth noting that these activation energy values are dependent on the nature of the assumed alkene-free intermediate.

As for the C_{2v}-symmetric models, the transition state for the *E* isomer insertion is higher in energy of nearly 5 kJ/mol relative to the transition state for the *Z* isomer insertion, compare top of the bars on the left in Figure 4. However, the corresponding activation energy calculated for the *E* isomer is lower of nearly 7 kJ/mol relative to that for the *Z* isomer, due to the deeper coordination energy for the *Z* isomer, compare the height of the bars on the left of Figure 4.

As for the C_s-symmetric models, the lower energy transition state (of nearly 5 kJ/mol) and the lower activation energy (of nearly 8 kJ/mol) correspond to the *E* isomer. In fact, for insertion steps corresponding to a *R* (*S*) chirality at the metal center the tail methyl group of the *re*−*re* (*si*−*si*) *E*-butene enantioface is on the opposite side with respect to the fluorenyl ligand (Figure 6B), while for the *Z* isomer the tail methyl group is at repulsive distance relative to one of the six-membered rings of the fluorenyl ligand (Figure 6A). Of course, for insertion steps corresponding to a *R* (*S*) chirality at the metal center, a high energy transition state and a high activation energy correspond to insertion of the *si*−*si* (*re*−*re*) enantioface of the *E* isomer. In fact, not only the tail methyl group but also the growing chain experiences repulsive van der Waals interactions with one of the six-membered rings of the fluorenyl ligand (Figure 6C).[58]

As for the C_2-symmetric models, the lower energy transition state (of nearly 12 kJ/mol) corresponds to the *Z* isomer (Figures 4 and 7). In fact, for the *Z* and *E* isomers the transition states presenting the growing chain in an unencumbered sector, and the head methyl group in a relative anti orientation with respect to the growing chain (Figure 7, parts A and B), present the tail methyl group on the opposite (Figure 7A) and on the same side (Figure 7B) with respect to one of the six-membered ring of the bis(indenyl) ligand, respectively. It is apparent from Figure 7B that for the catalytic complexes with a (*R*,*R*) coordination of the π ligand, the tail methyl group of the *re*−*re* enantiomer of the *E* isomer is at a repulsive distance with respect to one of the six-membered rings of the bis(indenyl) ligand. Moreover, the transition state for the insertion of the *si*−*si* enantioface of the *E* isomer presents the tail methyl group far from the indenyl ligand as well as the head methyl group far from the growing chain, but presents the growing chain on the same side of (and hence interacting with) the bis(indenyl) ligand (Figure 7C). Since the large energy difference between the transition states of the *E* isomer (with the *si*−*si* enantioface) and the *Z* isomer is close to the calculated coordination energy for the *Z* isomer, similar activation energies (close to 35 kJ/mol) have been evaluated (Figure 4).

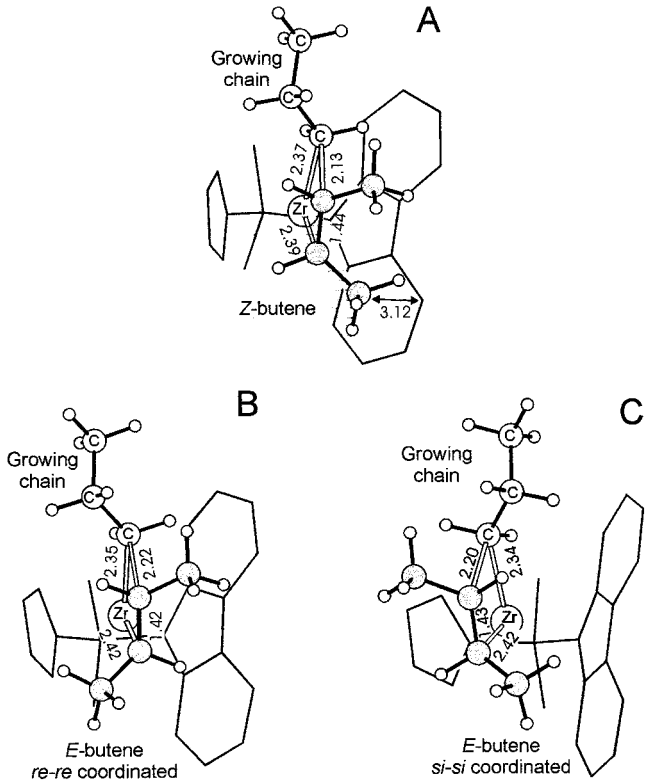

Figure 6. Transition states calculated for the C_s-symmetric metallocene for the step corresponding to the *R* chirality at the central metal atom, for *Z*-butene, A, and *E*-butene *re*−*re*, B, and *si*−*si* coordinated, C. The main bond distances, in Å, are indicated. The short nonbonded distance between the tail methyl group of the *Z* isomer and a carbon atom of the fluorenyl ligand is also indicated. The alkenes carbon atoms are shaded for clarity.

4. Polymerization Tests

Experimental Details. Polymerization grade ethene was purchased from Società Ossigeno Napoli and used without further purification. 2-Butenes were purchased from Aldrich. MAO was purchased from Witco and used as a solid after distillation of solvent. Toluene was refluxed over sodium diphenylketyl for 48 h and distilled before use. Dimethylsilylbis(cyclopentadienyl)$ZrCl_2$, ethenebis(1-indenyl)$ZrCl_2$ and isopropylidene(cyclopentadienyl)(9-fluorenyl)$ZrCl_2$ were synthesized according to the literature.[4,59,60]

Copolymerizations were carried out by the following general procedure: in a 50 mL glass flask, equipped with a magnetic stirrer, were introduced sequentially 7 mL of toluene, 5 mL of 2-butene, 565 mg of MAO dissolved in 9 mL of toluene, and 1×10^{-5} mol of metallocene dissolved in 1 mL of toluene. The flask was fed with a constant overpressure of ethene of 3 cm of paraffin−oil. After 48 h the polymerization was stopped by introducing a few milliliters of methanol; the mixture was poured into acidified ethanol. The polymer was

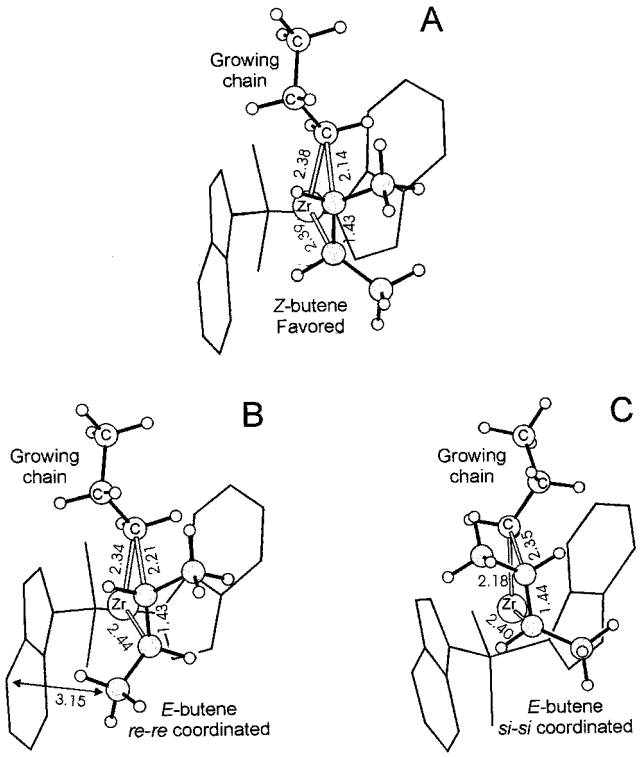

Figure 7. Transition states calculated for the C_2-symmetric metallocene presenting a (*R*,*R*) chirality of coordination of the bis(indenyl) ligand, for *Z*-butene, A, and *E*-butene *re*−*re*, B, and *si*−*si* coordinated, C. The main bond distances, in Å, are indicated. The short nonbonded distance between the tail methyl group of the *re*−*re* coordinated *E* isomer and a carbon atom of the indenyl ligand is also indicated. The alkenes carbon atoms are shaded for clarity.

recovered by filtration, washed with fresh ethanol, and dried in a vacuum at 60 °C.

NMR spectra were recorded on an AM 250 Bruker spectrometer operating at 62.89 MHz at 393 K. The samples were prepared by dissolving 40 mg of polymer in 0.5 mL of tetrachlorodideutero ethane. Hexamethyldisiloxane was used as internal chemical shift reference. The resonances were assigned as reported in Table 1 on the basis of the data reported in the literature for carbons in similar environments,[61] on the DEPT ^{13}C NMR experiment[62] and on additivity Grant and Paul rules.[63]

Copolymer compositions were calculated by summarizing the concentration of following resonances:

$$a = C_1 + C_2 + C_3 + C_4 + C_5 + \frac{1}{2}C_6 + \frac{1}{2}C_7 + C_{10} + C_{11} + \frac{1}{2}C_{12} + C_{21} + \frac{1}{2}C_{22}$$

$$b = C_9 + C_{15} + C_{19} + C_{24}$$

$$X_E = \frac{\frac{1}{2}a}{\frac{1}{2}a + b} \qquad X_B = \frac{b}{\frac{1}{2}a + b}$$

Polymerization Results. ^{13}C NMR spectra of ethene copolymers with *Z* and *E*-butene, obtained by the C_s-symmetric catalyst isopropyl(cyclopentadienyl)(9-fluorenyl)$ZrCl_2$ are shown in parts A and B of Figure 8, respectively, while those obtained by the C_2-symmetric catalyst ethenebis(1-indenyl)$ZrCl_2$ are shown in parts

Table 1. Chemical Shifts of the Carbon Atoms, Labeled According to Figures 8 and 9, of the Ethene/2-Butene Copolymers[a]

	chemical shifts δ in ppm		
carbons	observed	expected	ref
1	11.95	11.86	76
2	20.65	20.6	76
3	29.97	30.0	76
4	27.73	27.8	76
5	28.71	28.18	61
6	25.19	25.25	61
7	35.32	35.35	61
8	31.86	31.06	61
9	17.87	17.8	61
10	28.23	28.3	61
11	25.09	25.1	61
12	31.86	31.9	61
13	37.48	37.5	61
14	24.55	24.5	61
15	9.06	9.0	61
16	37.66	37.85	24
17	35.82	34.7−37.2	24
18	14.77	14.4−15.6	24
19	9.26	9.2	77
20	28.71	28.7	77
21	32.64	33.0	77
22	17.35	17.5	77
23	34.82	34.9	77
24	139.03	138.9	63, 76
25	17.92	17.9	24, 76
26	116.16	116.0	63, 76
27	11.27	11.1	63, 76
28	22.41	22.3	63, 76
29	32.37	32.3	63, 76

[a] Hexamethyldisiloxane was used as internal chemical shift reference.

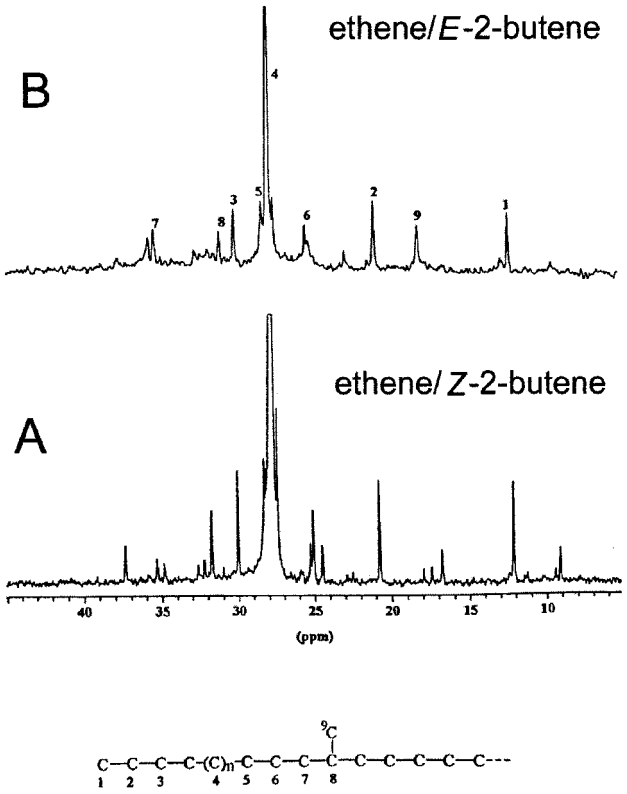

Figure 8. ^{13}C NMR spectra of ethene copolymers with *Z*−butene, A, and *E*-butene, B, obtained by the C_s-symmetric catalyst isopropyl(cyclopentadienyl)(9-fluorenyl)$ZrCl_2$, corresponding to runs 4 and 5 of Table 3, respectively. To show weak peaks, the spectra of parts A and B have been expanded by factors of 10 and 2, respectively. The chemical shift scale is in ppm downfield of HMDS. Relevant resonance attributions for the ethene/*E*-butene copolymer are explicitly indicated (see the annexed chain structure and Table 1).

Table 2. Ethene/2-butene Copolymerizations Performed in the Presence of the C_{2v}-Symmetric Catalyst Based on Dimethylsilylbis(cyclopentadienyl)$ZrCl_2$ and MAO

run	monomer	X_{im}[a]	X_{ie}[b]	T_{3-mb}[c]	T_{np}[d]	T_u[e]	X_E[f]	X_B[g]	$M_n \times 10^3$ [h]
1	*Z*-butene	0.01_5	0.01_4	0.00_6	0.01_5	traces	0.97_0	0.02_9	2.7
2	*E*-butene	0.07_1			0.11_1		0.92_8	0.07_1	0.5
3	2-butenes	0.02_2		traces	0.03_8		0.97_7	0.02_2	1.5
	Z 40% + *E* 60%								

[a] Molar fraction of isolated methyl groups. [b] Molar fraction of isolated ethyl groups. [c] Molar fraction of 3-methylbutyl end groups. [d] Molar fraction of *n*-propyl end groups. [e] Molar fraction of unsaturated end groups (3-methyl-2-butenyl). [f] Molar fraction of ethene in the copolymer. [g] Molar fraction of 2-butene in the copolymer. [h] Number-average molecular weight determined by end groups analysis.

Table 3. Ethene/2-Butene Copolymerizations Performed in the Presence of the C_s-Symmetric Catalyst Based on Isopropyl(cyclopentadienyl)(9-fluorenyl)$ZrCl_2$ and MAO

run	monomer	X_{im}[a]	X_{ie}[b]	T_{3-mb}[c]	T_{isob}[d]	T_{np}[e]	X_E[f]	X_B[g]	$M_n \times 10^3$ [h]
4	*Z*-butene	0.00_2	0.00_8	0.00_4		0.02_7	0.98_6	0.01_4	1.8
5	*E*-butene	0.14_2	traces	traces	0.00_2	0.10_0	0.85_6	0.14_4	0.6
6	2-butenes	0.00_8				0.00_6	0.99_2	0.00_8	9.4
	Z 40% + *E* 60%								

[a] Molar fraction of isolated methyl groups. [b] Molar fraction of isolated ethyl groups. [c] Molar fraction of 3-methylbutyl end groups. [d] Molar fraction of isobutyl end groups. [e] Molar fraction of *n*-propyl end groups. [f] Molar fraction of ethene in the copolymer. [g] Molar fraction of 2-butene in the copolymer. [h] Number-average molecular weight determined by end groups analysis.

Table 4. Ethene/2-Butene Copolymerizations Performed in the Presence of C_2-Symmetric Catalyst Based on Ethenebis(1-indenyl)$ZrCl_2$ and MAO

run	monomer	X_{vm}[a]	X_{im}[b]	X_{ie}[c]	$T_{3\text{-}mb}$[d]	T_{np}[e]	T_u[f]	X_E[g]	X_B[h]	$M_n \times 10^3$ [i]
7	*Z*-butene	0.00_9	0.01_5	0.19_6	0.02_0	0.00_7	0.01_3	0.74_6	0.25_3	2.6
8	*E*-butene		0.00_7			0.01_5		0.99_2	0.00_8	4.0
9	2-butenes	traces	0.01_9	0.04_6	0.00_7	0.02_0	0.01_0	0.91_8	0.08_1	2.3
	Z 40% + *E* 60%									

[a] Molar fraction of vicinal *erythro* methyl groups. [b] Molar fraction of isolated methyl side groups. [c] Molar fraction of isolated ethyl side groups. [d] Molar fraction of 3-methylbutyl end groups. [e] Molar fraction of *n*-propyl end groups. [f] Molar fraction of unsaturated end groups (3-methyl-2-butenyl). [g] Molar fraction of ethene in the copolymer. [h] Molar fraction of 2-butene in the copolymer. [i] Number-average molecular weight determined by end groups analysis.

A and B of Figure 9, respectively. On the basis of the relative intensities of the weak signals with respect to the predominant methylene signal of ethene sequences (at 27.7 ppm), it is immediately apparent that the amount of *Z*-butene and *E*-butene comonomers inserted into the polymer chain is much larger for the case of catalysts with C_2-symmetric and C_s-symmetric ligands, respectively.

As for the ethene/*E*-butene copolymer samples, the signals (Figures 8B and 9B) are due to isolated methyl groups in the polymer chain and to *n*-propyl end groups. More complex is the microstructure of the ethene/*Z*-butene copolymers (Figures 8A and 9A). In fact, besides weak signals equal to those observed for the ethene/*E*-butene copolymers, more intense signals corresponding to isolated ethyl groups are observed. It is also worth noting that a very weak peak corresponding to vicinal methyl groups in *erythro* configuration is also observed (Figure 9A).

As for the end groups, only *n*-propyl groups are substantially observed in ethene/*E*-butene copolymers while also 3-methylbutyl end groups and unsaturated 3-methyl-2-butenyl groups are observed in ethene/*Z*-butene copolymers. It is worth noting that also isobutyl end groups are observed in a detectable amount only in the ethene/*E*-butene copolymer being richest in 2-butene.

The molar fractions of vicinal methyl groups, of isolated methyl groups, of isolated ethyl groups, and of 3-methylbutyl, 3-methyl-2-butenyl, *n*-propyl. and isobutyl end groups are reported in Tables 2−4, for ethene/2-butene copolymerizations in the presence of C_{2v}, C_s, and C_2 catalytic systems, respectively. The columns of Tables 2−4 labeled as X_E and X_B report the molar fractions of ethene and 2-butene incorporated into the copolymer samples. As for the C_{2v}-symmetric catalytic

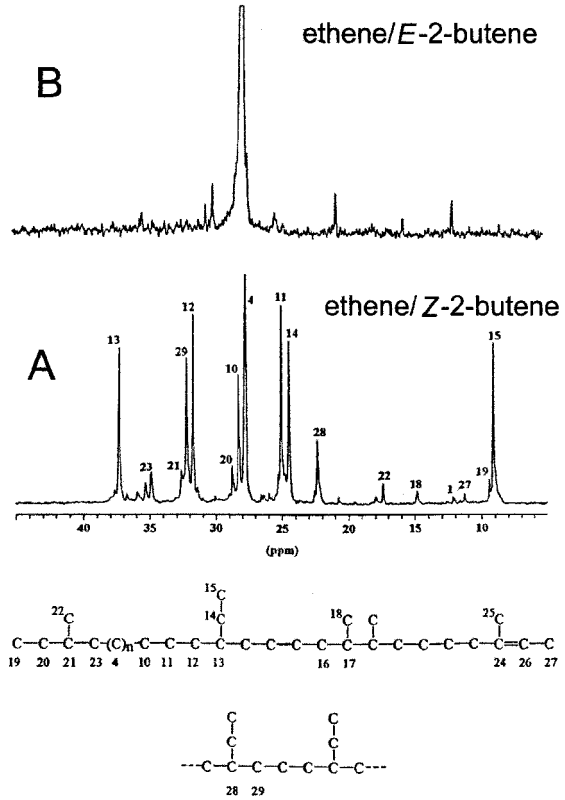

Figure 9. ^{13}C NMR spectra of ethene copolymers with *Z*−butene, A, and *E*-butene, B, obtained by the C_2-symmetric catalyst ethene-bis(1-indenyl)$ZrCl_2$, corresponding to runs 7 and 8 of Table 4, respectively. To show weak peaks, the spectra of parts A and B have been expanded by factors 2 and 10, respectively. The chemical shift scale is in ppm downfield of HMDS. Relevant resonance attributions for the ethene/*Z*-butene copolymer are explicitly indicated (see the annexed chain structures and Table 1).

Scheme 3

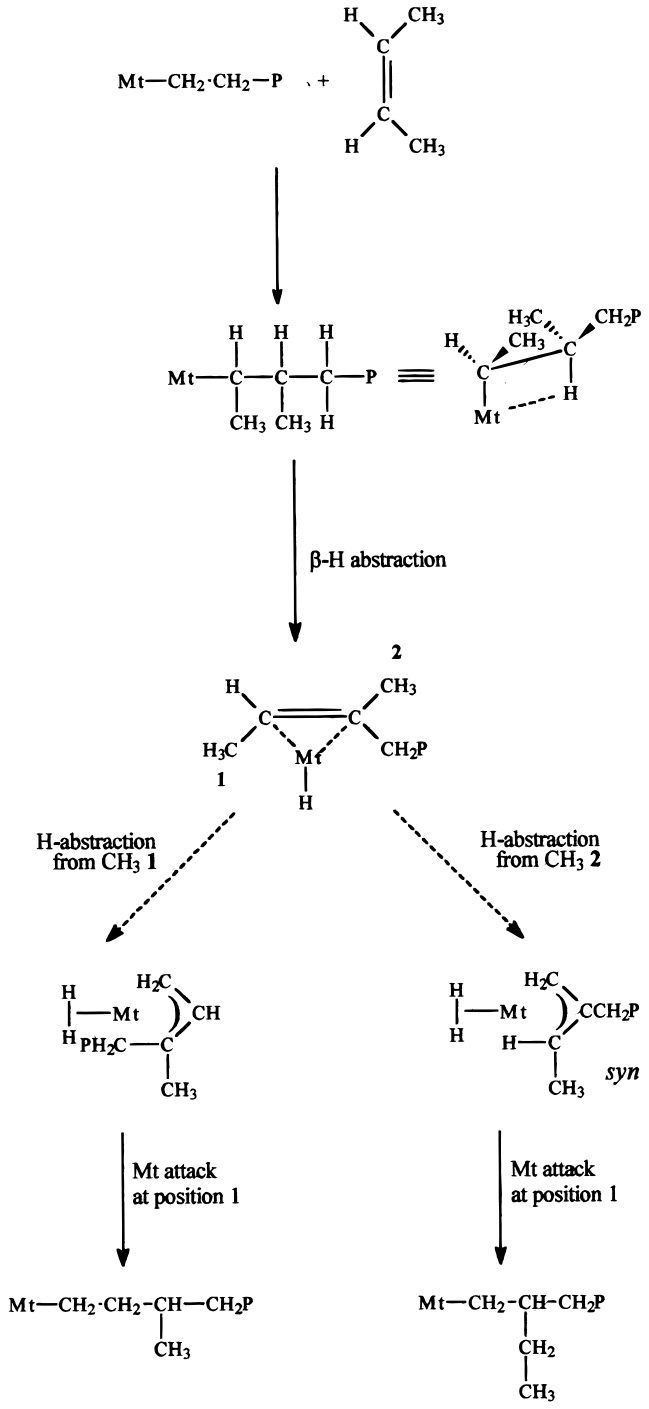

Scheme 4

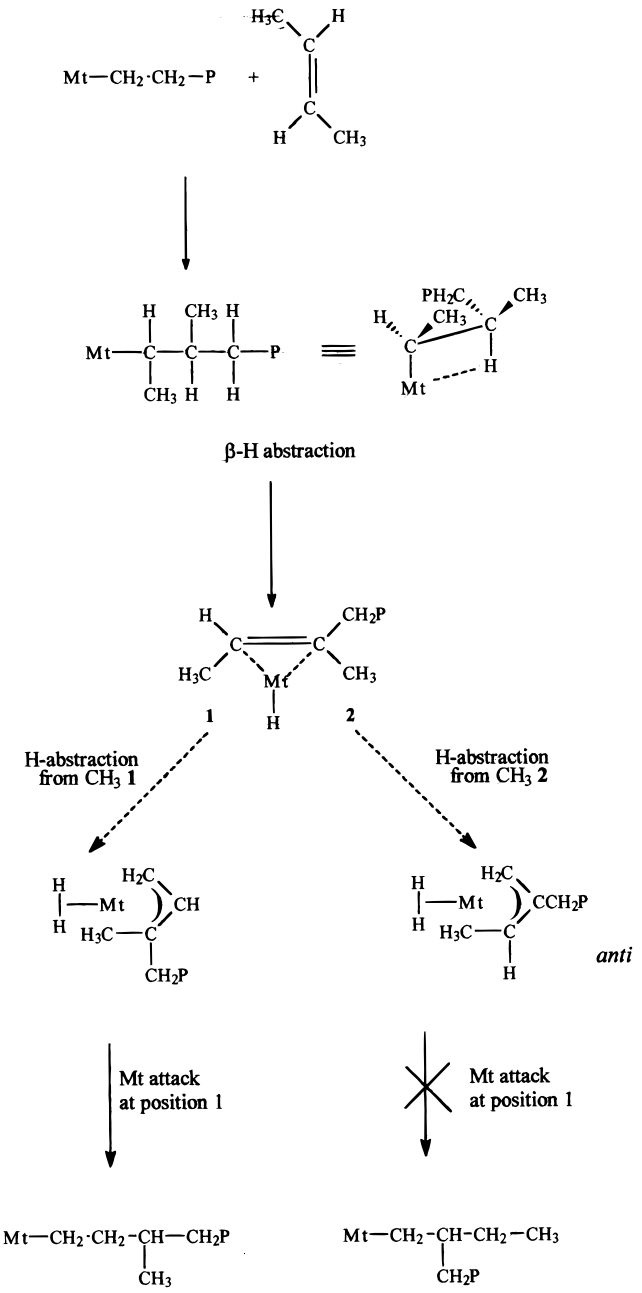

system, the X_B values of Table 2 show that the amounts of the 2-butene isomers copolymerized with ethene are closer to each other (with the *E* isomer nearly twice more abundant) than for C_s and C_2 catalytic systems (compare Figures 8 and 9 and Tables 3 and 4). Moreover, the isomerizations and end groups remain for both comonomers equal to those observed for both C_s and C_2 catalytic systems.

Beside data of polymerization runs for pure *Z*- and *E*-butene, also data for a mixture of them are reported (third rows of Tables 2−4). In the presence of C_{2v}- and C_s-symmetric catalysts (Tables 2 and 3), the prevailing constitution of the comonomeric units (isolated methyl groups) and of the end groups (*n*-propyl) are those typical of the *E*-butene. On the contrary, in the presence of the C_2-symmetric catalyst (Table 4), the prevailing constitution of the comonomeric units (isolated ethyl groups) and the presence of unsaturated end groups are typical of copolymerization of *Z*-butene. This confirms that *E*-butene is more reactive in the presence of C_{2v}- and C_s-symmetric catalysts while *Z*-butene is more reactive in the presence of the C_2-symmetric catalyst. Comparisons between X_B values of Tables 2 and 3 for pure *E* isomer and the mixture of *E* and *Z* isomers (runs 2 and 5 vs runs 3 and 6, respectively) show that the reactivity of *E*-butene, for both C_{2v}- and C_s-symmetric catalysts, is significantly reduced in the presence of the *Z* isomer.

The last columns of Tables 2−4 report the number-average molecular weights evaluated on the basis of the molar fraction of the end groups.

5. Discussion

Growing Chain Isomerizations. Independent of the symmetry of the catalytic systems, the obtained

Scheme 5

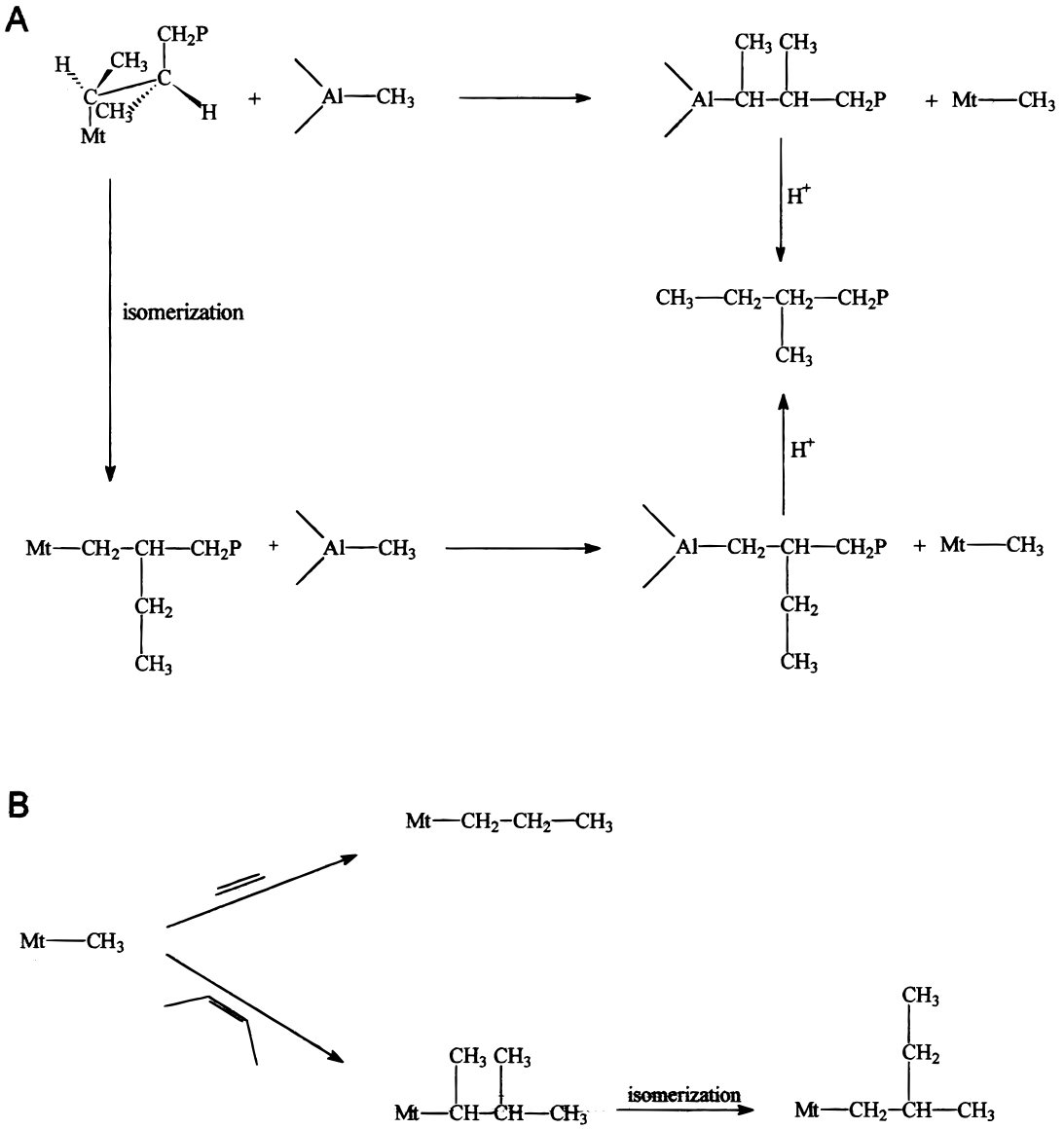

ethene/*E*-butene copolymers incorporate the comonomer units generating isolated methyl groups. These are reasonably produced by an isomerization reaction analogous to the well-known 3,1 isomerization reaction observed as a consequence of secondary monomer insertions,[24,64] for propene polymerization by several metallocene-based catalytic systems. In fact, in the vicinity of the catalytic metal atom, a 2-butene ending polymer chain, Mt−CH(CH_3)−CH(CH_3)−P, is similar to the growing polymer chain after a secondary propene insertion, Mt−CH(CH_3)−CH_2−P. Signals of vicinal methyl groups, which would correspond to 2-butene insertion in the absence of growing chain isomerization (see upper part of Scheme 3), are not observed.

On the other hand, independent of the symmetry of the catalytic systems, the obtained ethene/*Z*-butene copolymers incorporate the comonomer units generating prevailingly isolated ethyl groups. Hence, the largest fraction of *Z*-butene enters the polymer chain generating a comonomer unit identical to that one observed for 1-butene polymerization, possibly through an isomerization reaction of the 2-butene ending polymer chain which is different from that one observed for ethene/*E*-butene copolymerizations with the same systems. The vicinal methyl groups in *erythro* configuration, which are present in minor amounts, are those expected for *cis*-addition of *Z*-butene units (see upper part of Scheme 4), in the absence of isomerization.[65,66]

As for the isomerization mechanisms, the pathways which are tentatively proposed in Schemes 3 and 4 involve the formation of metal−allyl bonds, as suggested for different isomerization reactions which have been observed in alkene polymerizations by metallocenes.[67−70] In particular, it is tentatively suggested that pathways leading to isolated ethyl groups would involve the formation of syn (Scheme 3) or anti (Scheme 4) isomers of a same allyl group, when the last inserted monomer unit is *Z*- or *E*-butene, respectively. The higher energy of the anti allyl group could account for the absence of isolated ethyl groups for the *E*-butene copolymers. Molecular modeling analyses relative to these possible isomerization mechanisms, which could be also useful to rationalize the 3−1 isomerizations observed for propene polymerizations, are in progress.

Chain Transfer Reactions. As for ethene/*Z*-butene copolymerizations, chain transfer mechanisms well established for propene polymerization by metallocenes[71] are able to rationalize the observed end groups when

Scheme 6

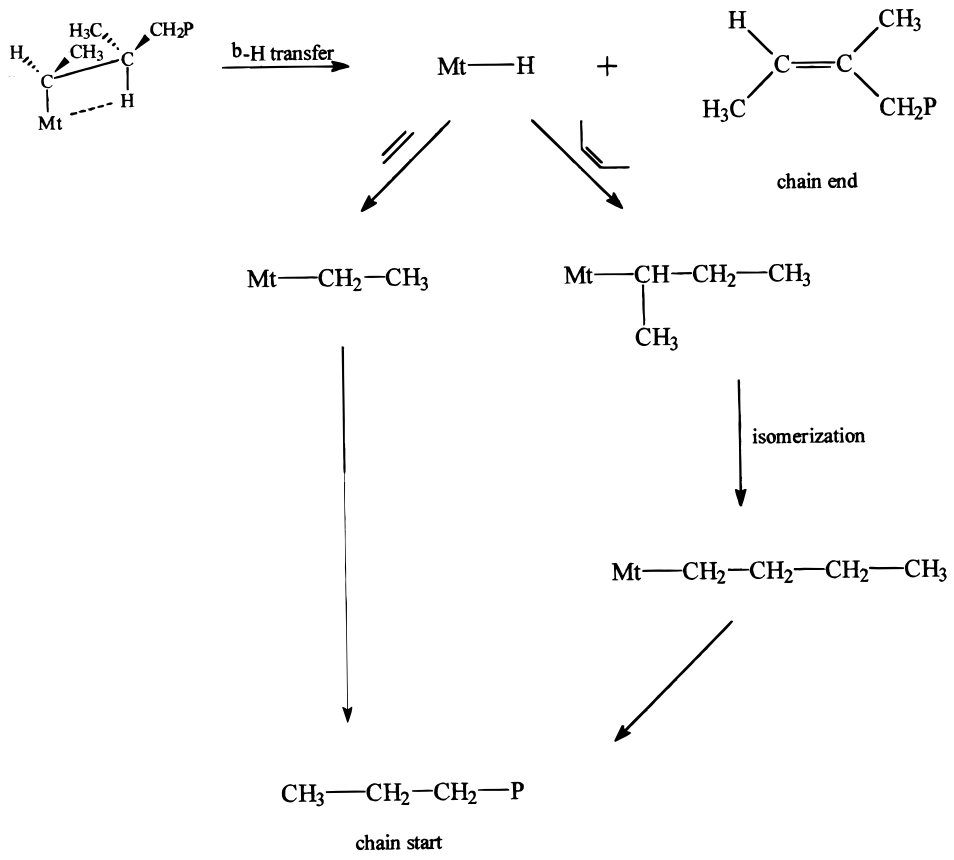

Scheme 7

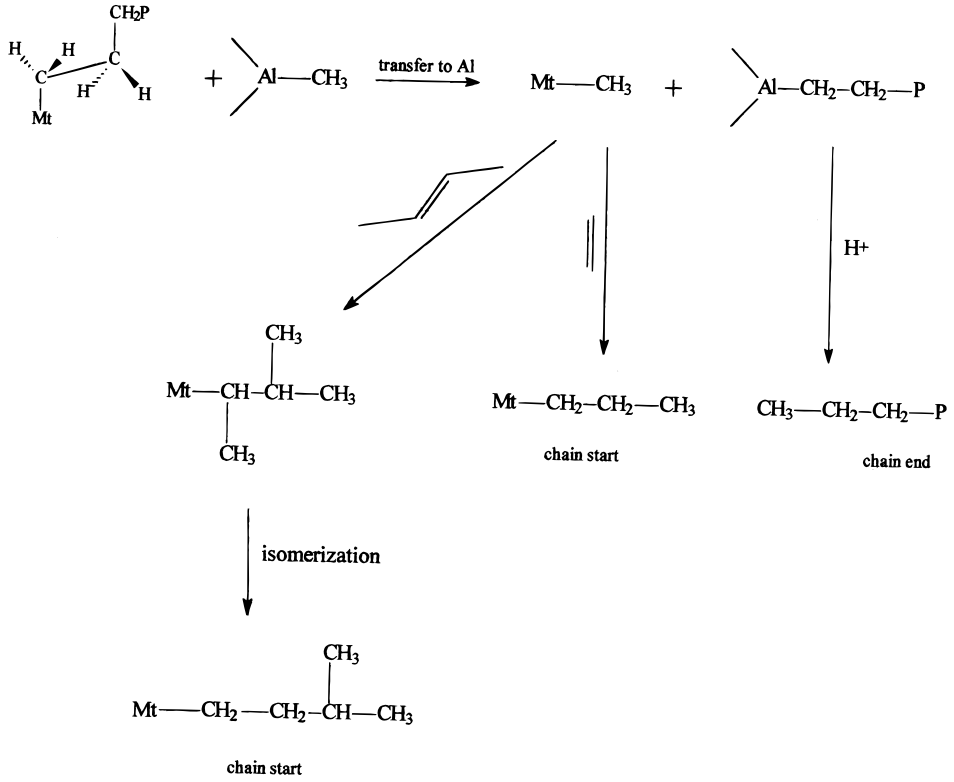

applied to catalytic models involving a 2-butene ending chain. In fact, the 3-methylbutyl end group is compatible with chain transfer of 2-butene ending chains to the aluminum cocatalyst,[72−75] as well as with a restart of the chain by 2-butene insertion into a metal−methyl bond, followed by the usual isomerization reaction. The same chain end would be observed if the transfer to aluminum would occur after the usual isomerization reaction of the *Z*-butene ending copolymer chain (Scheme 5).

Moreover, the 3-methyl-2-butenyl end group is compatible with β-hydrogen transfer to the transition metal from a 2-butene ending chain, before isomerization (Scheme 6). In this case, the restart of the chain by both ethene or 2-butene (followed by the usual isomerizations) insertions into a metal−hydride bond lead to formation of an *n*-propyl chain start (Scheme 6).

As for ethene/*E*-butene copolymerizations, the occurrence of *n*-propyl and minor amounts of isobutyl end groups is compatible with chain transfer of ethene ending chains to the aluminum cocatalyst and restart of the chain by ethene and 2-butene insertions into a metal−methyl bond (Scheme 7).

On the contrary, the well-established chain termination mechanisms (β-hydrogen transfer to the metal, β-hydrogen transfer to the monomer, transfer to the aluminum, and β-methyl transfer to the metal),[71] when applied to catalytic models involving 2-butene last inserted units, do not lead to formation of *n*-propyl groups. This suggests that, for the growing chain with *threo* configuration (following a *E*-butene insertion), chain transfer reactions such as those shown in Schemes 5 and 6 for the growing chain with the *erythro* configuration (following a *Z*-butene insertion), become less probable than ethene insertion.

Chain Propagation: Monomer Coordination and Insertion. The molecular modeling studies detailed in the first part of this paper have suggested and stimulated the experimental polymerization tests described in the second part of the paper, and have been able to predict the higher reactivity of *Z*-butene in the presence of C_2-symmetric catalysts and of *E*-butene in the presence of C_s-symmetric catalysts.

Moreover, a closer look to the energies of coordination intermediates and transition states, as well as to the activation energies relative to the insertion of both 2-butene isomers into ethene ending chains (Figure 4) allows a possible rationalization of other aspects of relative reactivities for these catalytic systems. In particular, for the C_{2v}-symmetric catalytic system the higher reactivity of the *E*-butene would be essentially related to its lower coordination ability, leading to lower activation energy for the insertion reaction. Moreover, the lower reactivity of *Z*-butene and of *E*-butene in the presence of the less hindered C_{2v} catalyst (first and second row of Table 2) as compared with the reactivity of the same monomers in the presence of more hindered C_s and C_2 catalysts (second row of Table 3 and first row of Table 4), is accounted for by higher activation energies. Finally, also the reduced reactivity of *E*-butene, for both C_{2v}- and C_s-symmetric catalyst, in the presence of the *Z* isomer (runs 3 and 6 vs runs 2 and 5) can be accounted for by the easier coordination of the less reactive *Z* isomer.

It is also worth noting that the present calculations suggest the presence of a substantial stereoselectivity for *E*-butene insertion for both C_s- and C_2-symmetric catalytic systems. This stereoselectivity is of course not relevant and not detectable for the presently considered catalytic systems whose maximum *E*-butene incorporation, mainly followed by isomerization leading to isolated methyl groups, is lower than 15% by mole.

Acknowledgment. The authors whish to thank Prof. Corradini of the University of Napoli, Prof. Zambelli of the University of Salerno, and Dr. Resconi of Montell Polyolefins for useful discussions. Financial assistance from the Italian Ministry for the University (PRIN 98), from the Italian National Research Council and from Montell Polyolefins is acknowledged.

References and Notes

(1) Ewen, J. A. *J. Am. Chem. Soc.* **1984**, *106*, 6355.
(2) Kaminsky, W.; Külper, K.; Brintzinger, H. H.; Wild, F. *Angew. Chem., Int. Ed. Engl.* **1985**, *24*, 507.
(3) Kaminsky, W. *Angew. Makromol. Chem.* **1986**, *145/146*, 149.
(4) Ewen, J. A.; Jones, R. L.; Razavi, A.; Ferrara, J. *J. Am. Chem. Soc.* **1988**, *110*, 6255.
(5) Ewen, J. A.; Elder, M. J.; Jones, R. L.; Haspeslagh, L.; Atwood, J. L.; Bott, S. G.; Robinson, K. *Makromol. Chem., Macromol. Symp.* **1991**, *48/49*, 253.
(6) Corradini, P.; Guerra, G.; Vacatello, M.; Villani, V. *Gazz. Chim. It.* **1988**, *118*, 173.
(7) Cavallo, L.; Guerra, G.; Vacatello, M.; Corradini, P. *Macromolecules* **1991**, *24*, 1784.
(8) Guerra, G.; Cavallo, L.; Moscardi, G.; Vacatello, M.; Corradini, P. *J. Am. Chem. Soc.* **1994**, *116*, 2988.
(9) Guerra, G.; Cavallo, L.; Moscardi, G.; Vacatello, M.; Corradini, P. *Macromolecules* **1996**, *29*, 4834.
(10) Corradini, P.; Cavallo, L.; Guerra, G. In *Metallocene Catalysts*; Kaminsky, W., Scheirs, J., Eds.; Wiley: New York, 2000; Vol. 2, p 3.
(11) Corradini, P.; Barone, V.; Fusco, R.; Guerra, G. *Eur. Polym. J.* **1979**, *15*, 133.
(12) Corradini, P.; Barone, V.; Guerra, G. *Macromolecules* **1982**, *15*, 1242.
(13) Zambelli, A.; Ammendola, P.; Grassi, A.; Longo, P.; Proto, P. *Macromolecules* **1986**, *19*, 2703.
(14) Zambelli, A.; Sacchi, M. C.; Locatelli, P.; Zannoni, G. *Macromolecules* **1982**, *15*, 211.
(15) Longo, P.; Grassi, A.; Pellecchia, C.; Zambelli, A. *Macromolecules* **1987**, *20*, 1015.
(16) Longo, P.; Proto, A.; Grassi, A.; Ammendola, P. *Macromolecules* **1991**, *24*, 4624.
(17) Pino, P.; Cioni, P.; Wei, J. *J. Am. Chem. Soc.* **1987**, *109*, 6189.
(18) Pino, P.; Galimberti, M.; Prada, P.; Consiglio, G. *Makromol. Chem.* **1990**, *191*, 1677.
(19) Cavallo, L.; Guerra, G.; Vacatello, M.; Corradini, P. *Chirality* **1991**, *3*, 299.
(20) Cossee, P. *J. Catal.* **1964**, *3*, 80.
(21) Arlman, E. J.; Cossee, P. *J. Catal.* **1964**, *3*, 99.
(22) Guerra, G.; Longo, P.; Cavallo, L.; Corradini, P.; Resconi, L. *J. Am. Chem. Soc.* **1997**, *119*, 4394.
(23) It is worth noting that the nonbonded interactions generating stereoselectivity are those between the methyl substituent of the coordinated propene and the chiral-oriented growing chain in the case of primary insertion and between the propene methyl group and one of the six-membered rings of the π-ligand in the case of secondary insertion.[22]
(24) Grassi, A.; Zambelli, A.; Resconi, L.; Albizzati, E.; Mazzocchi, R. *Macromolecules* **1988**, *21*, 617.
(25) Mizuno, A.; Tsutsui, T.; Kashiwa, N. *Polymer* **1992**, *33*, 254.
(26) Busico, V.; Cipullo, R.; Talarico, G.; Segre, A. L.; Caporaso, L. *Macromolecules* **1998**, *31*, 8720.
(27) (a) Caporaso, L.; Izzo, L.; Oliva, L. *Macromolecules* **1999**, *32*, 7323. (b) Caporaso, L.; Zappile, S.; Izzo, L.; Oliva, L. *Macromolecules*, submited.
(28) Natta, G.; Dall' Asta, G.; Mazzanti, G.; Pasquon, I.; Valvassori, A.; Zambelli, A. *J. Am. Chem. Soc.* **1961**, *83*, 3343.
(29) Corradini, P.; Ganis, P. *Makromol. Chem.* **1963**, *42*, 255.
(30) Kaminsky, W.; Bark, A.; Arndt, M. *Makromol. Chem. Macromol. Symp.* **1991**, *47*, 83.
(31) Guerra, G.; Longo, P.; Corradini, P.; Cavallo, L. *J. Am. Chem. Soc.* **1999**, *121*, 8651.
(32) Breslow, D. S.; Newburg, N. R. *J. Am. Chem. Soc.* **1959**, *81*, 81.
(33) Hanson, K. R. *J. Am. Chem. Soc.* **1966**, *88*, 2731.
(34) Cahn, R. S.; Ingold, C.; Prelog, V. *Angew. Chem., Int. Ed. Engl.* **1966**, *5*, 385.
(35) Prelog, V.; Helmchem, G. *Angew. Chem., Int. Ed. Engl.* **1982**, *21*, 567.
(36) Schlögl, K. *Top. Stereochem.* **1966**, *1*, 39.
(37) Stanley, K.; Baird, M. C. *J. Am. Chem. Soc.* **1975**, *97*, 6598.
(38) ADF 2.3.0 Vrije Universiteit Amsterdam: Amsterdam, The Netherlands, 1996.
(39) Baerends, E. J.; Ellis, D. E.; Ros, P. *Chem. Phys.* **1973**, *2*, 41.
(40) te Velde, B.; Baerends, E. J. *J. Comput. Phys.* **1992**, *99*, 84.

(41) Snijders, J. G.; Vernooijs, P.; Baerends, E. J. *At. Nucl. Data Tables* **1981**, *26*, 483.
(42) Vernooijs, P.; Snijders, J. G.; Baerends, E. J. Vrije Universiteit Amsterdam: Amsterdam, The Netherlands, 1981.
(43) Vosko, S. H.; Wilk, L.; Nusair, M. *Can. J. Phys.* **1980**, *58*, 1200.
(44) Becke, A. *Phys. Rev. A* **1988**, *38*, 3098.
(45) Perdew, J. P. *Phys. Rev. B* **1986**, *33*, 8822.
(46) Perdew, J. P. *Phys. Rev. B* **1986**, *34*, 7406.
(47) Cavallo, L.; Woo, T. K.; Ziegler, T. *Can. J. Chem.* **1998**, *76*, 1457.
(48) Woo, T. K.; Cavallo, L.; Ziegler, T. *Theor. Chem. Acc.* **1998**, *100*, 307.
(49) Deng, L.; Woo, T. K.; Cavallo, L.; Margl, P.; Ziegler, T. *J. Am. Chem. Soc* **1997**, *119*, 6177.
(50) Maseras, F.; Morokuma, K. *J. Comput. Chem.* **1995**, *16*, 1170.
(51) Doman, T. N.; Hollis, T. K.; Bosnich, B. *J. Am. Chem. Soc.* **1995**, *117*, 1352.
(52) Brooks, B. R.; Bruccoleri, R. E.; Olafson, B. D.; States, D. J.; Swaminathan, S.; Karplus, M. *J. Comput. Chem.* **1983**, *4*, 187.
(53) Rix, F. C.; Brookhart, M.; White, P. S. *J. Am. Chem. Soc.* **1996**, *118*, 4746.
(54) Musaev, D. G.; Froese, R. D. J.; Svensson, M.; Morokuma, K. *J. Am. Chem. Soc.* **1997**, *119*, 367.
(55) Margl, P. M.; Deng, L.; Ziegler, T. *Organometallics* **1998**, *17*, 933.
(56) Lohrenz, J. C. W.; Woo, T. K.; Ziegler, T. *J. Am. Chem. Soc.* **1995**, *117*, 2793.
(57) Yoshida, T.; Koga, N.; Morokuma, K. *Organometallics* **1995**, *14*, 746.
(58) For insertion of the *si*−*si* enantioface of the *E* isomer on the model site of R chirality, a similar energy transition state (not shown) presents a relative *syn* orientation of the head methyl group of butene and of the second carbon atom (and followings) of the growing chain, with both groups on the opposite side with respect to the fluorenyl ligand. This transition state relaxates the interactions of the growing chain with the fluorenyl ligand but presents substantial interactions between the growing chain and the head methyl group of butene.
(59) Wild, F.; Wasiucionek, M.; Huttner, G.; Brintzinger, H. H. *J. Organomet. Chem.* **1985**, *288*, 63.
(60) Bajgur, C. S.; Tikkamen, W. R.; Peterson, J. L. *Inorg. Chem.* **1985**, *224*, 2539.
(61) De Pooter, M.; Smith, P. B.; Dohrer, K. K.; Bennett, K. F.; Meadows, M. D.; Smith, C. G.; Schouwenaars, H. P.; Geerards, R. A. *J. Appl. Polym. Sci.* **1991**, *42*, 399.
(62) Pretsch, E.; Furst, A.; Badertscher, M.; Burgin, R.; Munk, M. E. *J. Chem. Inf. Comput. Sci.* **1992**, *32*, 291.
(63) Grant, D. M.; Paul, E. G. *J. Am. Chem. Soc.* **1964**, *86*, 2984.
(64) Soga, K.; Shiono, T.; Takemura, S.; Kaminsky, W. *Makromol. Chem., Rapid Commun.* **1987**, *8*, 305.
(65) Zambelli, A.; Giongo, M. G.; Natta, G. *Makromol. Chem.* **1968**, *112*, 183.
(66) Longo, P.; Grassi, A.; Proto, A.; Ammendola, P. *Macromolecules* **1988**, *21*, 24.
(67) Richardson, D. E.; Alameddin, N. G.; Ryan, M. F.; Hayes, T.; Eyler, J. R.; Siedle, A. R. *J. Am. Chem. Soc.* **1996**, *118*, 11244.
(68) Margl, P. M.; Woo, T. K.; Blöchl, P. E.; Ziegler, T. *J. Am. Chem. Soc* **1998**, *120*, 2174.
(69) Karol, F. J.; Kao, S.; Wasserman, E. P.; Brady, R. C. *New J. Chem.* **1997**, *21*, 797.
(70) Resconi, L. *Polym. Mater. Sci. Eng.* **1999**, *80*, 421.
(71) Resconi, L.; Camurati, I.; Sudmeijer, O. *Top. Catal.* **1999**, *7*, 145.
(72) Chien, J. C. W.; Kuo, C. I. *J. Polym. Sci., Part A: Polym. Chem.* **1986**, *24*, 1779.
(73) Chien, J. C. W.; Wang, B. P. *J. Polym. Sci., A: Polym. Chem.* **1988**, *26*, 3089.
(74) Chien, J. C. W.; Razavi, A. *J. Polym. Sci., A: Polym. Chem.* **1988**, *26*, 2369.
(75) Resconi, L.; Bossi, S.; Abis, L. *Macromolecules* **1990**, *23*, 4489.
(76) Aubert, P.; Sledz, J.; Schvé, F.; Brevard, C. *J. Polym. Sci., Polym. Chem. Ed.* **1981**, *19*, 955.
(77) Cheng, H. N.; Smith, D. A. *Macromolecules* **1986**, *19*, 2065.

MA992186W